Journal of Geography and Cartography (2021) Volume 4 Issue 1
doi:10.24294/jgc.v4i1.1313

ORIGINAL RESEARCH ARTICLE

Integrating optical and microwave satellite observations for high resolution soil moisture estimate and applications in CONUS drought analyses

Donglian Sun[1*], Yu Li[1], Xiwu Zhan[2], Chaowei Yang[1], Ruixin Yang[1]

[1] *Dept. of Geography and Geoinformation Science, George Mason University, Fairfax, VA 22030, USA. E-mail: dsun@gmu.edu*

[2] *NOAA/NESDIS Center for Satellite Applications and Research, College Park, MD 20742, USA.*

Abstract

In this study, optical and microwave satellite observations are integrated to estimate soil moisture at the same spatial resolution as the optical sensors (5km here) and applied for drought analysis in the continental United States. A new refined model is proposed to include auxiliary data like soil texture, topography, surface types, accumulated precipitation, in addition to Normalized Difference Vegetation Index (NDVI) and Land Surface Temperature (LST) used in the traditional universal triangle method. It is found the new proposed soil moisture model using accumulated precipitation demonstrated close agreements with the U.S. Drought Monitor (USDM) spatial patterns. Currently, the USDM is providing a weekly map. Recently, "flash" drought concept appears. To obtain drought map on daily basis, LST is derived from microwave observations and downscaled to the same resolution as the thermal infrared LST product and used to fill the gaps due to clouds in optical LST data. With the integrated daily LST available under nearly all weather conditions, daily soil moisture can be estimated at relatively higher spatial resolution than those traditionally derived from passive microwave sensors, thus drought maps based on soil moisture anomalies can be obtained on daily basis and made the flash drought analysis and monitoring become possible.

Keywords: Soil Moisture; High Spatial Resolution; Regional Drought; Microwave and Optical Satellite Remote Sensing

ARTICLE INFO

Article history:
Received 15 February 2021
Accepted 29 March 2021
Available online 10 April 2021

1. Introduction

Drought is considered to be the most severe natural hazard in terms of impact, duration, and spatial extent[1]. The sparse spatial distribution of weather stations makes it daunting for drought monitoring and predicting. Satellite remote sensing capabilities have been greatly improved for decades and served as the main method for drought monitoring. Drought may occur unnoticeably and varyingly. Lack of information to drought may lead to severe disaster. The damage was extensive and the impact to livestock and farm production is uncountable[2].

Government agencies within National Oceanic and Atmospheric Administration (NOAA) and United States Department of Agriculture (USDA) have teamed up with the National Drought Mitigation Center (NDMC) to produce a weekly drought monitor (DM) map that incorporates climate data and professional input from all levels and is well known as the U.S. Drought Monitor (USDM). The USDM maps are consensus product based on several indicators and key variables, and the final maps are adjusted manually by numerous experts throughout the country to reflect the real-world conditions as reported[3]. The

USDM drought conditions are classified into five classes based on a ranking percentile approach: (1) D0 - abnormally, (2) D1 - moderate, (3) D2 - severe, (4) D3 - extreme, and (5) D4 - exceptional dry conditions. They are utilized as (1) D0-D4 (percentile ≤30%), (2) D1-D4 (percentile ≤20%), (3) D2-D4 (percentile ≤10%), (4) D3-D4 (percentile ≤5%), and (5) D4 (percentile ≤2%)[3–5].

The USDM maps are currently distributed online (http://droughtmonitor.unl.edu/) with relatively coarse resolution. They served as one of the criteria to determine the eligibility for relief of aggravation due to drought condition.

Agricultural interest in drought is important in much of the U.S. In fact, there is considerable interest in indices that can monitor agricultural drought. The hydrological condition of agricultural drought is closely linked to soil moisture[6], which is dependent on precipitation, water infiltration, and soil water holding capacity. Since it's hard to measure soil moisture over large area directly, Leese *et al*. concluded it's better to monitor soil moisture with combination of in-situ model and remote sensed variables respond to soil moisture[7]. Satellite remote sensing data with large area coverage is a promising and economical tool to estimate soil moisture and enables drought monitoring based on surface parameters, such as NDVI, LST, evaportranspiration, and soil moisture. The microwave-optical/IR synergistic approach is an efficient method to improve the current drought-related soil moisture products with several advantages including higher spatial and temporal resolutions. Zhan *et al*. described a synergistic technique using optical/infrared frequency products to overcome the coarse spatial resolution of the MW satellite products[8]. This method was later enhanced by Chauhan *et al*.[9]. They built the statistical relationships between near-surface soil moisture and optical-derived soil moisture indices. Merlin *et al*. applied these relations and transferred this method to a wider range of conditions[10]. However, this method requires many surface parameters and micrometeorological data, which may not be available over large areas. It's desirable to find a simple and reasonable model for drought monitoring comparable to the USDM drought classifications, and to explore the possibility for linking a real-time index with surface wetness condition in a fine resolution. In this study, a new approach to build a drought indicator at fine resolution are implemented with near real time microwave and optical satellite observations. After introduction of the study area and data used, specifics of these approaches and their results in analyzing drought conditions in the continental United States (CONUS, the latitude and longitude range is about 20 ~ 50 °N, and -125° ~ -75 °W) during the recent years are presented in the following sections.

2. Materials and methods

2.1 Data used

A comprehensive data set is collected and processed for deriving soil moisture at optical sensor resolution (5 km in this study) from satellite observations and evaluating drought conditions in the CONUS. These data include:

- MODIS LST and emissivity daily L3 global climate modeling grid (CMG) product (short name: MYD11C1) with a resolution of 0.05°[11].

- MODIS LST/emissivity 8-Day L3 CMG product (short name: MYD11C2) with a resolution of 0.05°[11].

- NDVI data is extracted from the MODIS 16-day composite NDVI product (short name: MYD13C1) with a resolution of 0.05°[12].

- Precipitation data are obtained from the TRMM (Tropical Rainfall Measuring Mission) Multi-satellite Precipitation Analysis (TMPA) with 0.25° spatial resolution and 3-hourly temporal resolution[13].

- Elevation data are derived from the National Elevation Dataset (NED) data at a resolution of 100 meters[14].

- MODIS land cover Climate Modeling Grid (CMG) product (Short Name: MCD12C1) provides the dominant land cover types at a spatial resolution of 0.05°.

- Soil texture data, including sand and porosity, are obtained from the Food and Agriculture Organization/United Nations Educational, Scientific and

Cultural Organization (FAO/UNESCO) soil map, with a resolution of about 0.0833°[15,16].

- Soil moisture data used for calibration is obtained from the Soil Moisture Operational Product System (SMOPS) at 0.25° resolution developed by NOAA-NESDIS. This SMOPS product merges soil moisture retrievals from microwave satellite sensors such as the Advanced Scatterometers (ASCAT) on MetOp-A and B, Soil Moisture and Ocean Salinity of European Space Agency, WindSat of Naval Research Lab based on the Single Channel Algorithm[17,18].

- Soil moisture outputs at 0.125° resolution from the three land-surface models (LSMs): the community Noah[19], the Mosaic[20], and the Variable Infiltration Capacity (VIC) model[21], are obtained from the North American Land Data Assimilation System (NLDAS)[22].

2.2 Temporal compositing and spatial resampling

The datasets used in this study were obtained at different temporal and spatial resolutions. All the datasets were needed to be resampled to the same resolution.

- For calibration using the SMOPS soil moisture (SM) data, all the datasets were aggregated to 25 km, the same resolution as the SMOPS SM data. The SM models were firstly built at 25 km resolution, then were applied to optical sensor data to estimate SM at the optical sensor resolution (5 km here).

- In order to compare with the USDM drought condition maps, all the datasets have been resampled or interpolated to uniform weekly (7 days) temporal and 0.0833° (about 12 km) spatial resolutions.

- For "flash" drought study, all the datasets were resampled or downscaled to the same 5 km spatial resolution as the MODIS LST product and estimate SM at 5 km spatial resolution on daily basis.

Land cover data has been resampled via the nearest neighbor assignment due to its discrete value. The bicubic interpolation assignment[23] was used to re-scale the other datasets, assuming that each point value changes consistently during observations.

2.3 Methods

2.3.1 A new model for high resolution soil moisture estimate

A close relationship exists between vegetation vigor and soil moisture availability, especially in arid and semiarid areas, thus in many cases satellite derived NDVI and LST products have been used to evaluate drought condition. Carlson *et al*. found the relationship between measured surface temperature, vegetation fraction, and soil moisture, known as the "Universal Triangle Model"[24]. Chauhan *et al*. argued that the second or third order polynomial gives a better representation of the data since a single polynomial represents a wide range of surface climate conditions and land surface types[9]. Thus a Universal Triangle Model was developed and can be described as:

$$\begin{aligned} SM = {} & a_{00} + a_{10} NDVI^{*} + a_{20} NDVI^{*2} \\ & + a_{01} LST^{*} + a_{02} LST^{*2} \\ & + a_{11} NDVI^{*} LST^{*} + a_{22} NDVI^{*2} LST^{*2} \\ & + a_{12} NDVI^{*} LST^{*2} + a_{21} NDVI^{*2} LST^{*} \end{aligned} \quad (1)$$

where $NDVI^{*} = \frac{NDVI - NDVI_{\min}}{NDVI_{\max} - NDVI_{\min}}$, $LST^{*} = \frac{LST - LST_{\min}}{LST_{\max} - LST_{\min}}$, subscripts max and min refer to the maximum and minimum values. Parameters a_{00}, a_{10}, …, a_{22} are the regression coefficients.

Sun and Kafatos[25] indicated the negative or reverse relation between NDVI and LST can only hold during warm or growing seasons, therefore, NDVI and LST related drought indices may only be used during warm seasons, but not winter. Chauhan *et al*. added surface albedo into the Universal Triangle Model to strengthen the relationship between soil moisture and measurable land surface parameters[9]. Nevertheless, surface types vary significantly, and therefore, even a combination of NDVI, LST or albedo is not enough to fully describe the surface conditions. Soil moisture is also highly related to precipitation (the land water balance equation indicates the change of soil moisture is highly related to precipitation), soil texture (physical properties such as dielectric constant can affect water content in soil), topography (runoff is highly related to the topographic position, slope aspect, and steepness), and

land cover (different land cover will influence the hydrological processes differently). LC data are numerical values. According to the product user guide (https://lpdaac.usgs.gov/sites/default/files/public/product_documentation/mcd12_user_guide_v6.pdf), the LC value range is from 1–17 and is assigned as: Evergreen Need leaf Forest as 1, Evergreen Broadleaf Forests as 2, Deciduous Needleleaf Forests as 3, Deciduous Broadleaf Forests as 4, Mixed Forests as 5, Closed Shrublands as 6, Open Shrublands as 7, Woody Savannas as 8, Savannas as 9, Grasslands as 10, Permanent Wetlands as 11, Croplands as 12, Urban and Built-up Lands, Cropland/Natural Vegetation Mosaics as 14, Permanent Snow and Ice as 15, and Barren as 16, and Water Bodies as 17. Thus it is desirable to combine and integrate all these datasets to build a soil moisture model as:

$$SM = b_0 + b_1 NDVI^* + b_2 NDVI^{*2} + b_3 LST^* + b_4 \,\mathrm{Pr} + b_5 DEM + b_6 Sand + b_7 Poro + b_8 LC \quad (2)$$

where "Pr" represents precipitation, "*DEM*" is for Digital Elevation Model (DEM) data, "*Sand*" is the individual grains or particles which can be seen with the naked eyes, "*Poro*" refers to porosity about how many pores/holes a soil has, and "*LC*" is for land cover data. b_0, b_1, …, b_8 are regression coefficients.

As shown in **Figure 1**, the black line in Figure 1b is the corresponding normalized monthly accumulated precipitation, and the LOWESS (Locally Weighted Scatterplot Smoothing)[26] is applied to describe the nonlinear trends of precipitation (the blue line in **Figure 1b**). The drought condition may not be directly reflected by temporal variation in precipitation because drought is caused by precipitation deficit during some period of time, usually more than a season. It is found that precipitation has an accumulating and lagging effect on drought condition. For example, the trend of precipitation is reduced in 2006 and 2011 (**Figure 1b**), yet the USDM drought maps marked these years as normal conditions (**Figure 1a**) due to sufficient accumulated rainfall in previous period. While in 2014, the precipitation had increasing trend, but short of accumulated rainfall from the previous period in 2013 and early 2014, thus the USDM classified year 2014 as drought condition. This result demonstrated that the accumulated precipitation from the last year's warm season to the current time can describe the drought conditions better than the daily precipitation. Therefore, a refined soil moisture model is proposed by using the accumulated precipitation starting from the last year's warm season. The refined soil moisture model can be described as:

$$SM = c_0 + c_1 NDVI^* + c_2 NDVI^{*2} + c_3 LST^* + c_4 \, Ac\_\mathrm{Pr} + c_5 DEM + c_6 Sand + c_7 Poro + c_8 LC \quad (3)$$

where Ac_Pr is for the accumulated precipitation starting from April of the previous year until the requested day, all other variables are the same as Equation (2). c_0, …. c_8 are the regression coefficients.

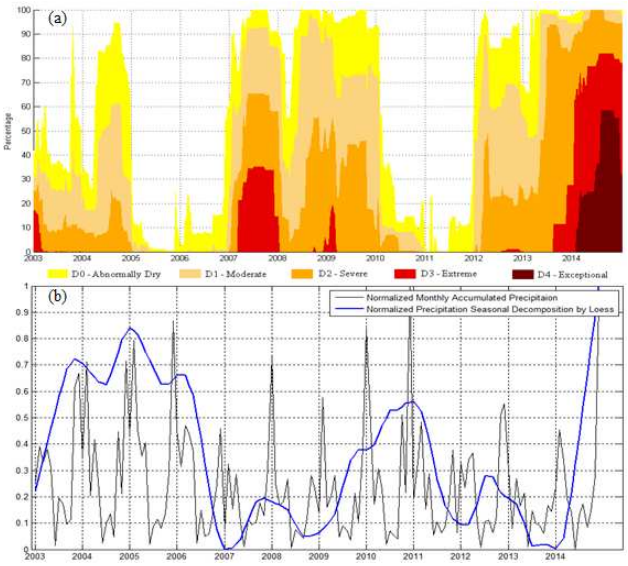

Figure 1. (a) The USDM weekly drought condition map; (b) normalized monthly accumulated precipitation over California (32 - 42 °N, 114 - 125 °W) retrieved from the TRMM, and normalized monthly accumulated precipitation seasonal decomposition by the LOWESS (blue line), from Jan. 2003 to Dec. 2014.

The SMOPS soil moisture products were used for calibration to derive the regression coefficients in Equations (1), (2), and (3). The least square regression was applied to estimate the regression coefficients and 50% data were used for training.

2.3.2 Anomaly calculation

Soil moisture changes slowly, therefore cannot catch the fast change of drought conditions. Soil moisture anomaly is more appropriate to describe

drought conditions than the absolute soil moisture[27]. In this study, we averaged daily soil moisture into weekly to match with the UM drought maps temporally. Soil moisture anomaly maps are obtained by the difference between weekly soil moisture and the long-term average soil moisture based on the equation:

$$SM\_Anomaly = SM - \overline{SM} \quad (4)$$

where the average soil moisture $\overline{SM}$ for each pixel is calculated for the same weeks over the 11 years from January 1 2003 to December 31 2014. Negative soil moisture anomalies stand for the observed data are lower than the averaged data, and indicate dry conditions.

2.3.3 Comparison with some other drought indices

- Evaporative Stress Index (ESI)

The ESI is defined as the anomalies in the ratio of actual-to-potential ET (AET/PET), derived from the thermal remote sensing based on the Atmosphere-Land Exchange Inverse (ALEXI) surface energy balance model[28–31]. The ALEXI uses measurements of morning land-surface temperature retrieved from geostationary satellite thermal band imagery to solve the Two-Source Energy Balance (TSEB) algorithm[32] in time-differential model. Actual ET (AET) output from the ALEXI is estimated as the potential ET (PET) expected under non-moisture limiting conditions, yielding a non-dimensional ET variable, ESI, ranging from 0 (dry) to approximately 1 (wet).

- Vegetation Health Index (VHI)

Kogan *et al*. proposed to combine the Vegetation Condition Index (VCI) and the Temperature Condition Index (TCI) to Vegetation Health Index (VHI)[33]:

$$VHI = a * VCI + b * TCI \quad (5)$$

where the coefficient a and b are usually taken as 0.5. The VCI is defined as:

$$VCI = \frac{NDVI - NDVI_{min}}{NDVI_{max} - NDVI_{min}} \quad (6)$$

where $NDVI_{max}$ and $NDVI_{min}$ are the multi years maximum and minimum $NDVI$ in a given area for growing season. The TCI is defined by Kogan[34] as:

$$TCI = 100 \times (BT_{max} - BT_i)/(BT_{max} - BT_{min}) \quad (7)$$

where BT, BT_{max}, and BT_{min} are smoothed brightness temperature, its maximum and minimum, respectively calculated for each pixel and week from multiyear data, and i is the year.

The Center for Satellite Applications and Research (STAR) of NOAA Satellite and Information Service (NESDIS) is providing global VCI, TCI, and VHI map every week at: http://www.star.nesdis.noaa.gov/smcd/emb/vci/VH/vh_browse.php.

- Vegetation Temperature Condition Index (VTCI)

Wang *et al*. developed Vegetation Temperature Condition Index (VTCI) based on the triangular space of LST and NDVI for monitoring drought stress[35]. It's defined as following:

$$VTCI = \frac{LST_{NDVIi.max} - LST_{NDVIi}}{LST_{NDVIi.max} - LST_{NDVIi.min}} \quad (8)$$

where $LSTNDVI_{i.max}$ and $LSTNDVI_{i.min}$ are the maximum and minimum land surface temperature of pixels which have the same $NDVI_i$ value, respectively, $LSTNDVI_i$ denotes land surface temperature of one pixel whose $NDVI$ value is $NDVI_i$. If $VTCI(i) < 0.4$, then the area (i) is under severe drought condition.

2.3.4 Correlation analyses

The temporal correlation coefficients are computed between the outputs from the refined soil moisture model and the USDM drought classifications at weekly scales during the growing season from April to October of each year.

3. Results

Figure 2 demonstrates drought conditions over the contiguous U.S. based on soil moisture anomalies (the first 8 rows) and percentiles (bottom) derived from the refined model and compared with the USDM drought maps (the first row), the VTCI (the second row), the VHI (the third row), the ESI (the fourth row), and soil moisture anomalies from the Mosaic LSM (the five row), the community Noah LSM (the six row), and the VIC LSM (the seven row) for drought conditions from 2005 to 2010 (6 years).

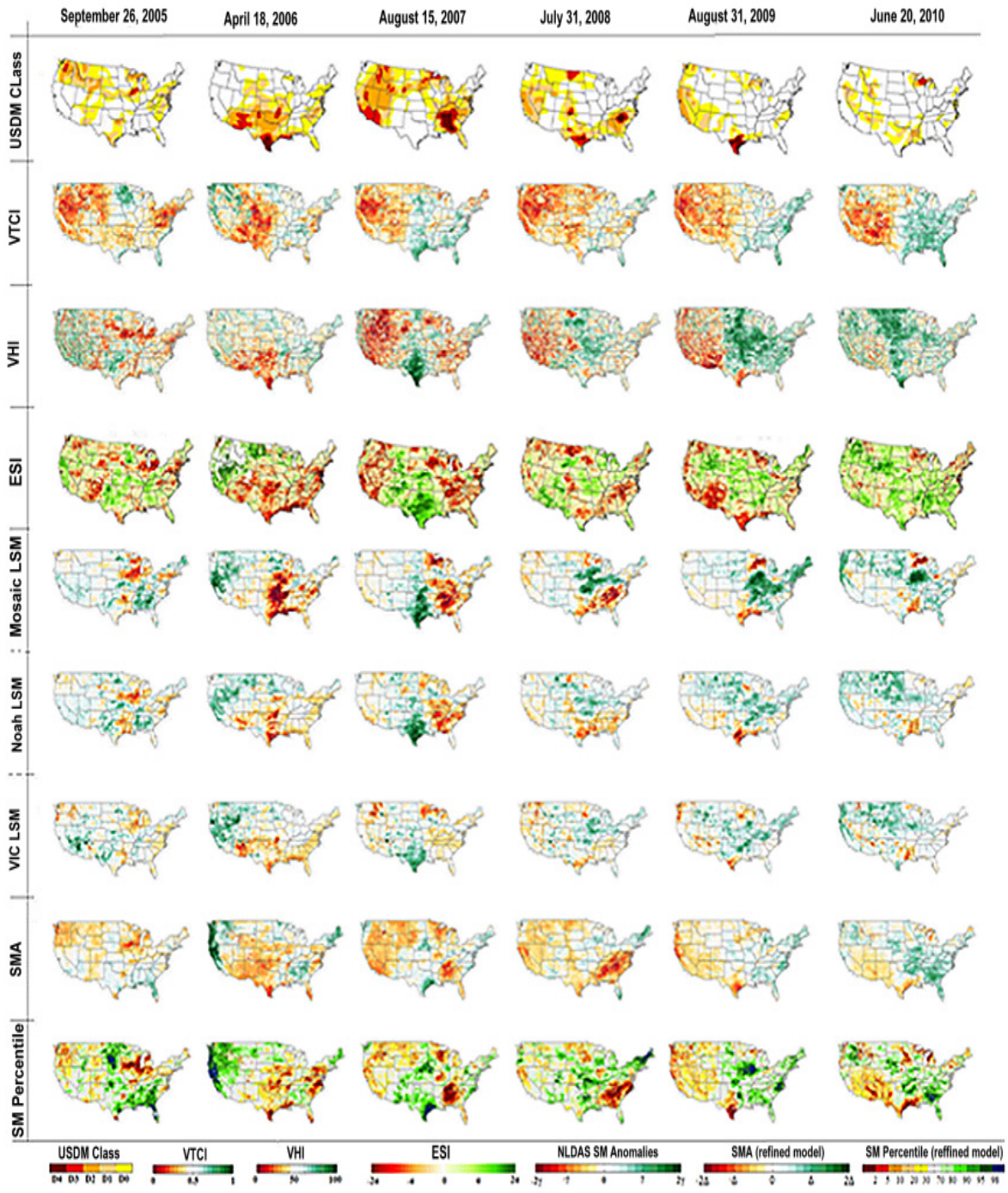

Figure 2. Drought conditions in the contiguous U.S. from different indicators. From top to bottom: the USDM classification (top), VTCI (the 2nd), VHI (the third), ESI (the fourth), the Mosaic LSM (the five), the Noah LSM (the sixth), the VIC LSM (the seventh), soil moisture anomalies based on the refined model (the eighth), and the soil moisture percentile (the bottom) based on the refined model. The three LSMs (Mosaic, Noah, and VIC) share the same color palette**.**

It is found the percentile of soil moisture cannot easily catch the fast changes, so percentile of soil moisture anomalies is used instead. The VHI and ESI show good agreements with the USDM classifications, while the NLDAS three LSM outputs demonstrate similar patterns. The soil moisture derived from the proposed soil moisture model provides an easy way for monitoring surface drought conditions,

and the surface dry/wetness patterns agree with the USDM classifications.

Figure 3 shows the temporal correlation coefficients between the soil moisture anomalies derived from the refined model and the USDM drought classes during different years from 2005 to 2010, where greener color indicates a better agreement between the two classifications. In general, the refined soil moisture model outputs have high correlations with the USDM drought classifications. The statistical metrics of Averaged Temporal Correlation Coefficients are also listed in **Table 1**. In general, the basic model with the introduction of soil texture data show improvement to the triangle model, while the refined model outputs have higher correlation with the USDM drought classifications and show further improvement to the basic model.

Recently, "flash" drought concept appears. Flash drought frequently occurred in the central and eastern United States[36]. The 2012 drought over the Northern American demonstrated the worst surface condition since the 1930s Dust Bowl[37]. The drought started in 2011, extended rapidly in 2012 (especially in June and July according to the USDM classifications), and continued in 2013. This event was pervasive in the central regions of the United

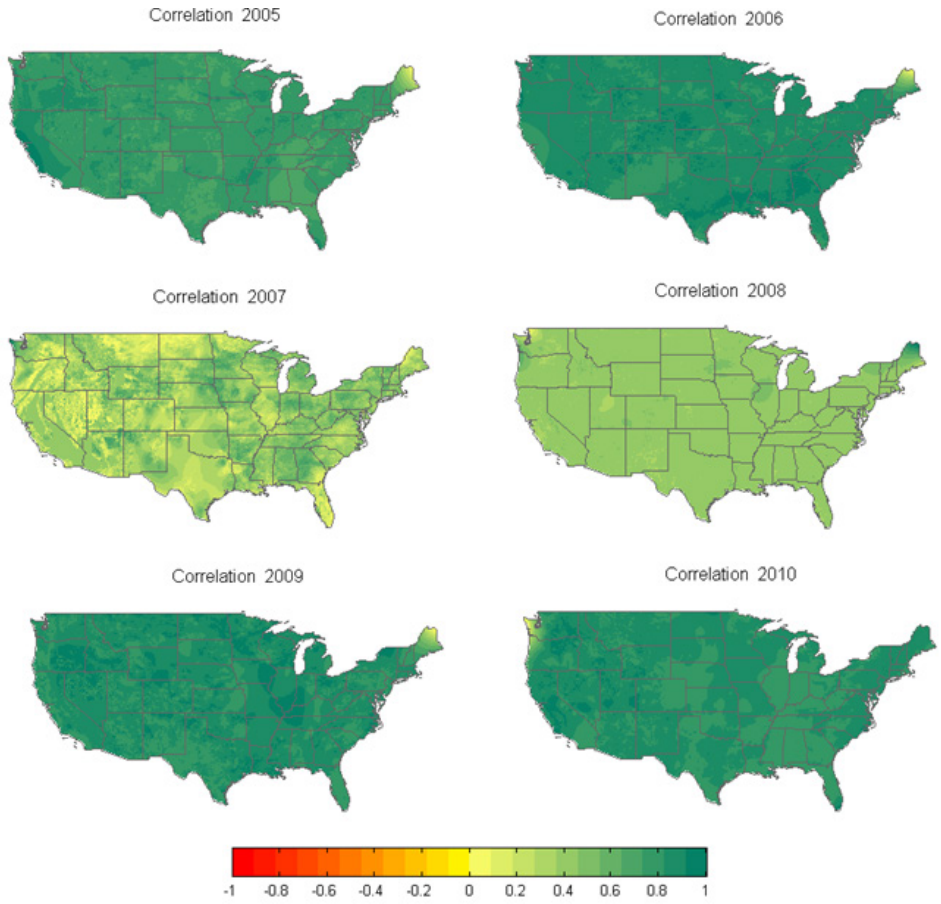

Figure 3. The temporal correlation coefficient maps between the refined soil moisture model outputs and the USDM drought classifications during different years**.**

Table 1. The statistical metrics of Averaged Temporal Correlation Coefficients between the soil moisture outputs from the three different models and USDM classifications

SM models\years	2005	2006	2007	2008	2009	2010
Triangle model	0.245	0.548	0.105	0.219	0.460	0.298
Basic model	0.672	0.720	0.382	0.557	0.486	0.423
Refined model	0.748	0.773	0.599	0.618	0.766	0.759

States due to the absence of rainfall in the growing season. The rapid soil moisture loss led this event as "flash drought"[38]. Unlike the common drought that is caused by external forcing like SST anomalies, the flash drought event was a result of natural weather variations, with little warnings found from the traditional drought metrics or climate model simulations[39]. The flash drought event suggests that the current drought monitoring should enhance its temporal resolution.

In the above drought analyses as shown in **Figure 2** and **Figure 3**, the LST input to the soil moisture model is the weekly composite data. Because thermal infrared (TIR) LST can only be obtained under clear conditions, as shown in **Figure 4a**, there are a lot of gaps or missing values due to clouds in the daily MODIS LST. Only weekly composite can get a clear LST map. Since microwave sensor can penetrate most non-rainy clouds and observe the Earth surface, so we think about using microwave observations to fill the gaps due to clouds in the thermal IR LST. The microwave observations will be firstly calibrated to thermal IR (MODIS here) LST, and then downscaled to the same spatial resolution as the TIR LST, and then merged with the TIR observations to fill the gaps due to clouds in the TIR LST. The detailed information and processes are described in another paper[40]. Here we show an example in **Figure 4**. As demonstrated in **Figure 4**, the original daily MODIS LST exist a lot of gaps due to clouds (**Figure 4a**), while the LST derived from the AMSR-E with a new proposed five-channel algorithm[40] can get a clear and spatial continuous distribution (**Figure 4b**). **Figure 4c** is the merged MODIS and AMSR-E LST by using the AMSR-E to fill the gaps in the MODIS LST, and **Figure 4d** shows the integrated MODIS and AMSR-E LST by applying the geographically weighted regression (GWR) method to downscale the AMSR-E LST to the same MODIS resolution and further fill the pass gaps in the AMSR-E observations. With the integrated MODIS and AMSR-E LST, spatial continuous LST on a daily basis can be input into the proposed refined SM model to obtain soil moisture anomaly every day. The flow chart of the process is shown in **Figure 5**.

The USDM as well as other drought indicators

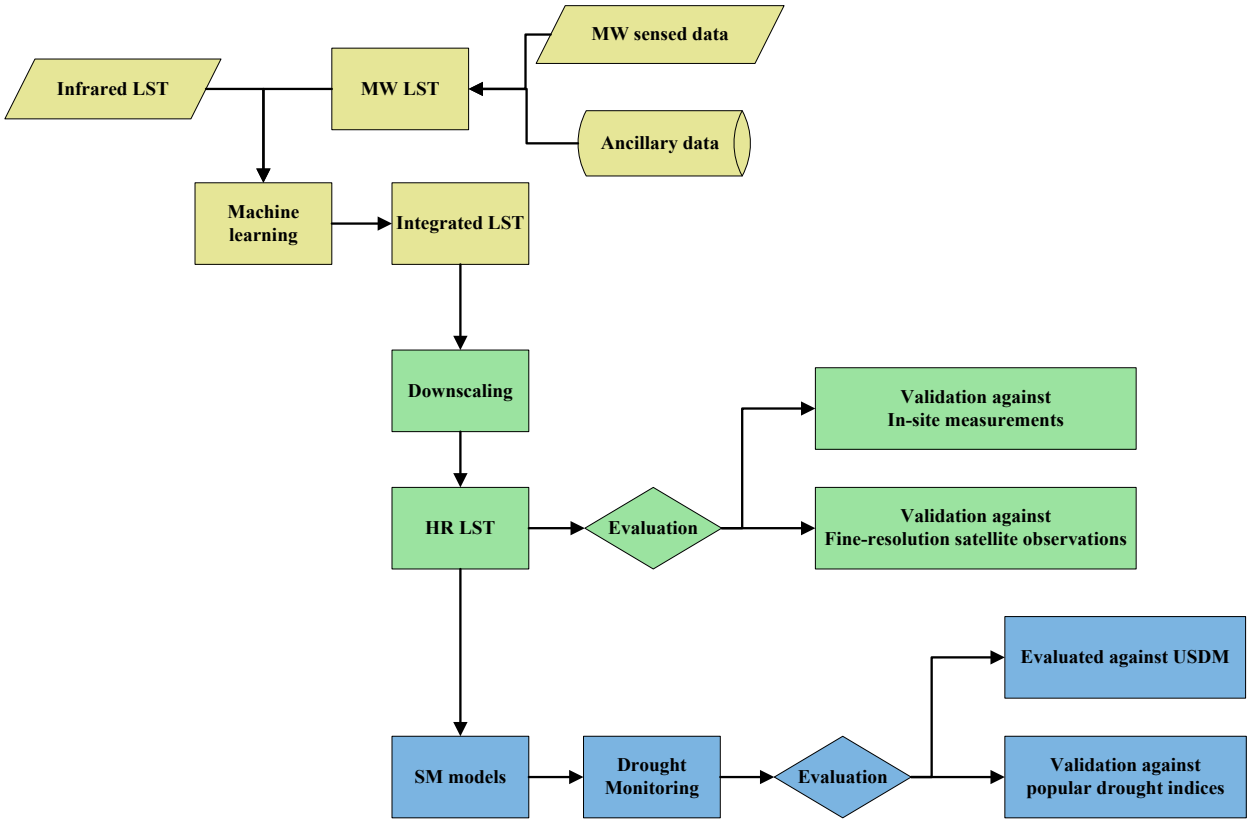

Figure 5. The flow-chart for soil moisture estimate and application in drought analysis.

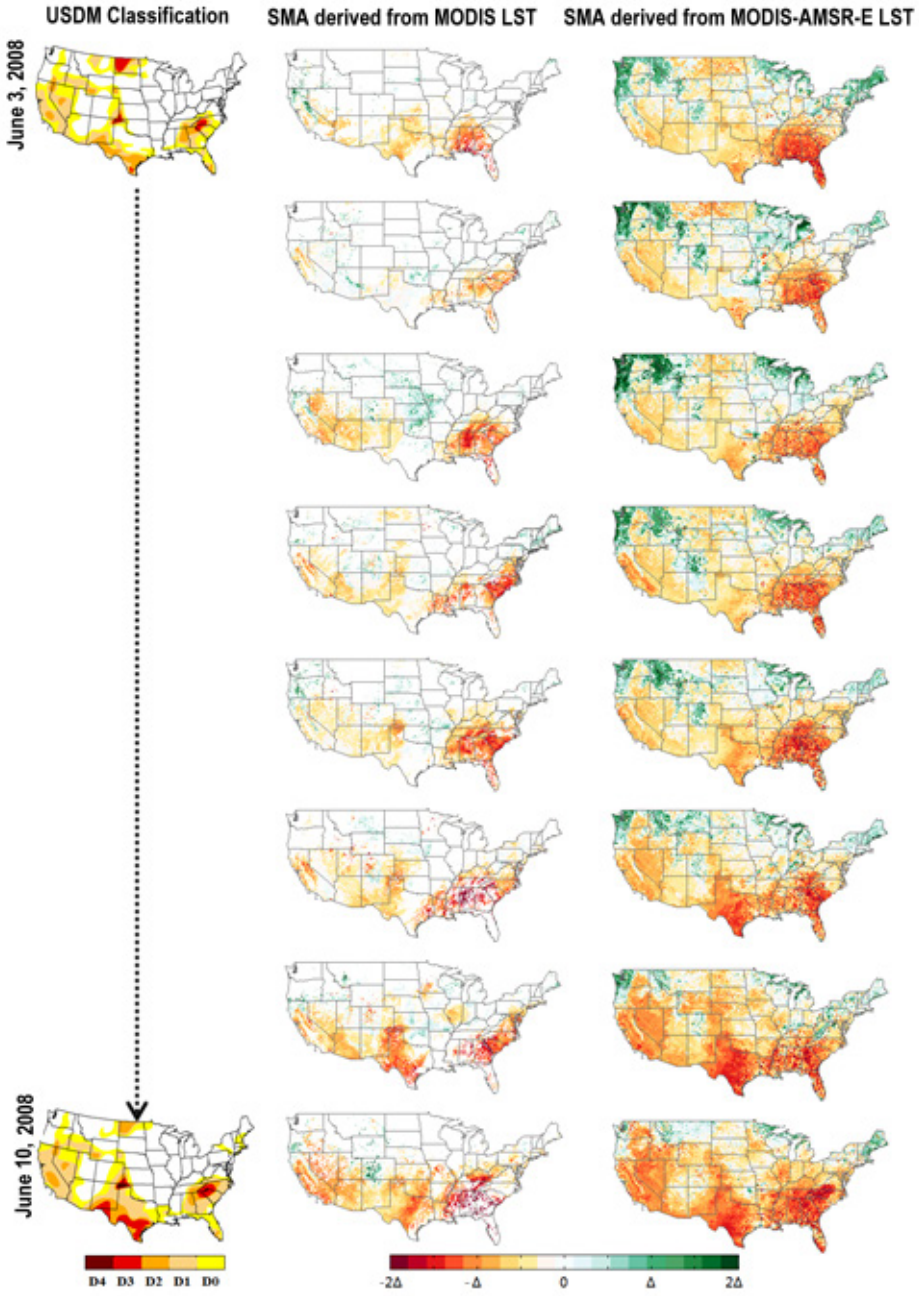

Figure 6. An example of daily SM anomalies compared with the weekly USDM drought map**.** First column: weekly USDM observations. Soil moisture anomalies observations in the continuous 8 days (from June 3 to June 10); second column: based on previous LST and third column: based on the new derived Example-based LST. Δ equals to 0.02 (unit: m3m-3).

can provide a weekly drought monitoring, while the new algorithm can provide soil moisture anomaly observations on a daily basis. The previous LST product that input into the soil moisture model is lack of observations due to clouds, and made the observation of soil moisture anomalies with gaps (**Figure 6**, the second column, white area is lack of observation, thus is considered as in the normal surface condition). With the TIR and microwave integrated LST, daily soil moisture anomalies can be obtained continuously without gaps (**Figure 6**, the third column). It matches with the USDM drought maps, and meanwhile catches the flash changes of dought conditions.

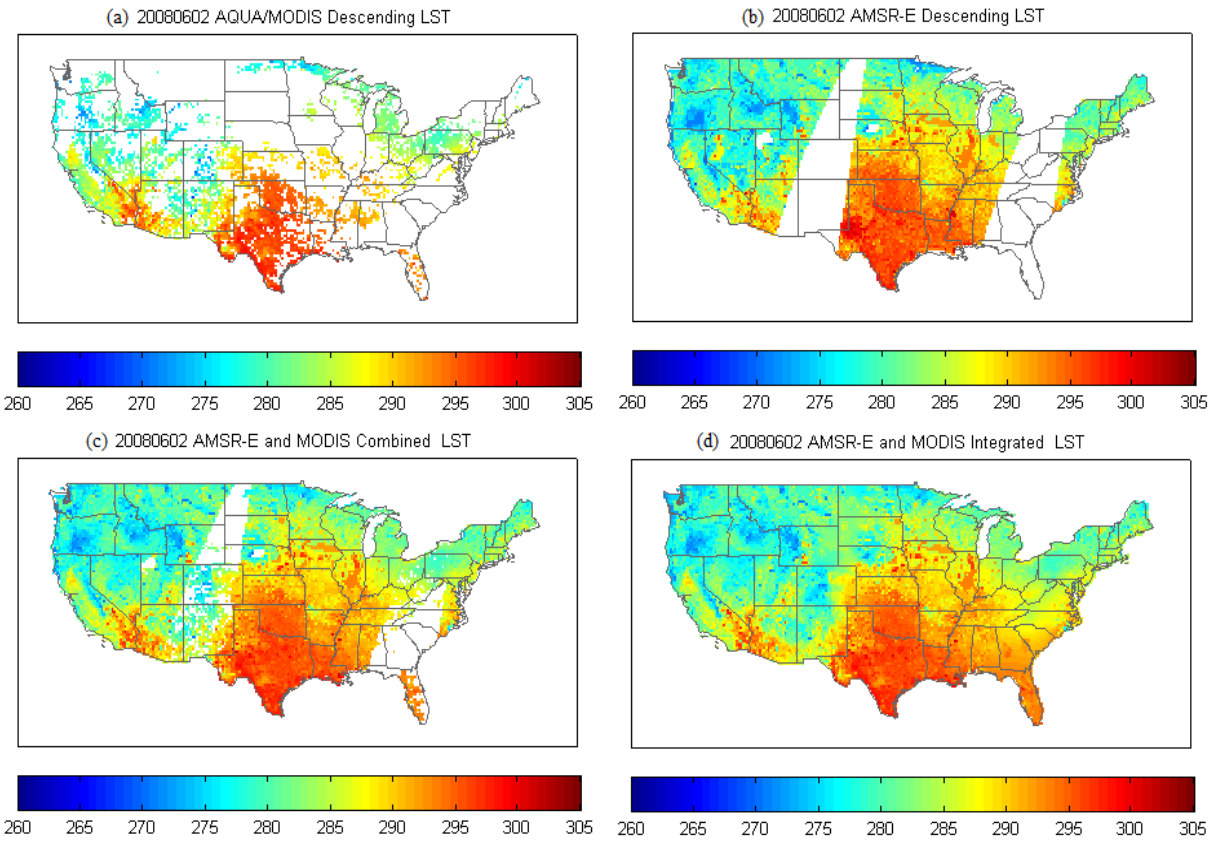

Figure 4. (a) Cloud free MODIS LST at 5 km resolution; (b) the derived AMSR-E LST at 25 km resolution; (c) the merged MODIS and AMSR-E LST at 25 km resolution; (d) the integrated LST from MODIS and AMSR-E with the GWR-based method applied to fill the gaps and also downscale to the same 5 km resolution as the MODIS LST, during daytime on June 2, 2008.

4. Discussion and conclusion

In this study, we integrated microwave and optical sensors to estimate soil moisture at high spatial resolution and used them to evaluate drought conditions in the continental United States. A new model is proposed to estimate soil moisture with the auxiliary data such as precipitation, topography, soil texture, and surface types, in addition to LST and NDVI used in traditional universal triangle model. We further applied the LOWESS model based on time series analysis, and found precipitation had some kind of accumulated and lagging effects on soil moisture, therefore we proposed to use accumulated precipitation starting from last year's warm season, instead of daily precipitation. The drought conditions identified by the soil moisture anomalies derived from the proposed model show close agreement with the USDM classifications.

There are still some limitations in this study: (1) this application was limited to the warm season, while cold season needs further investigation to fulfill the requirement of surface monitoring; (2) to further improve the applications, more agricultural related data should be examined. Since our model output can also provide the information of wetness level, agricultural related data such as irrigation, should be used as an important evaluation for the outputs.

Conflict of interest

The authors declare that they have no conflict of interest.

Acknowledgments

The work is supported by NOAA under grant# NA12NES4400006. The manuscript's contents are solely the opinions of the authors and do not constitute a statement of policy, decision, or position on behalf of NOAA or the U.S. Government.

References

1. Kousky C. Informing climate adaptation: A review of the economic costs of natural disasters. Energy Economics 2014; 46: 576–592.
2. Wilhite DA, Glantz MH. Understanding: The drought phenomenon: the role of definitions. Water International 1985; 10(3): 111–120.
3. Svoboda M, LeComte D, Hayes M, *et al*. The drought monitor. Bulletin American Meteorological Society 2002; 83(8): 1181–1190.
4. Mote PW. Climate-driven variability and trends in mountain snowpack in Western North America. Journal of Climate 2006; 19(23): 6209–6220.
5. Xia YL, Ek MB, Peters-Lidard CD, *et al*. Application of USDM statistics in NLDAS-2: Optimal blended NLDAS drought index over the continental United States. Journal of Geophysical Research-Atmosphere 2014; 119(6): 2947–2965.
6. Bolten JD, Crow WT, Zhan XW, *et al.* Evaluating the utility of remotely sensed soil moisture retrievals for operational agricultural drought monitoring. IEEE Journal of Selected Topics in Applied Earth Observation and Remote Sensing 2010; 3(1): 57–66.
7. Leese J, Jackson T, Pitman A, *et al.* Meeting summary: GEWEX/BAHC international workshop on soil moisture monitoring, analysis, and prediction for hydrometeorological and hydroclimatological applications. Bulletin of American Meteorological Society 2001; 82(7): 1423–1430.
8. Zhan X, Miller S, Chauhan N, *et al.* Soil moisture visible/infrared radiometer suite algorithm theoretical basis document. Lanham, MD: Raytheon Syst. Company; 2002.
9. Chauhan NS, Miller S, Ardanuy P. Spaceborne soil moisture estimation at high resolution: a microwave-optical/IR synergistic approach. International Journal of Remote Sensing 2003; 24(22): 4599–4622.
10. Merlin O, Walker JP, Chehbouni A, *et al.* Towards deterministic downscaling of SMOS soil moisture using MODIS derived soil evaporative efficiency. Remote Sensing Environment 2008; 112(10): 3935–3946.
11. Wan ZM, Dozier J. A generalized split-window algorithm for retrieving land-surface temperature from space. IEEE Transactions on Geoscience and Remote Sensing 1996; 34(4): 892–905.
12. Huete A, Justice C, Van Leeuwen W. MODIS vegetation index (MOD13): Algorithm theoretical basis document. 1999.
13. Huffman GJ, Bolvin DT, Nelkin EJ, *et al*. The TRMM multisatellite precipitation analysis (TMPA): Quasi-global, multiyear, combined-sensor precipitation estimates at fine scales. Journal of Hydrometeorology 2007; 8 (1): 38–55.
14. Gesch D, Oimoen M, Greenlee S, *et al*. The national elevation dataset. Photogrammetric Engineering and Remote Sensing 2002; 68(1): 5–32.
15. Henkel M. 21st century homestead: Sustainable agriculture I. Lulu. com.; 2015. p. 98–103.
16. Batjes NH. A world dataset of derived soil properties by FAO–UNESCO soil unit for global modelling. Soil Use and Management 1997; 13(1): 9–16.
17. Jackson TJ. III. Measuring surface soil moisture using passive microwave remote sensing. Hydrological Processes 1993; 7(2): 139–152.
18. Zhan X, Liu J, Zhao L, *et al.* Soil moisture operational product system (SMOPS): Algorithm theoretical basis document. 2011.
19. Ek MB, Mitchell KE, Lin Y, *et al*. Implementation of Noah land surface model advances in the National Centers for Environmental Prediction operational mesoscale Eta model. Journal of Geophysical Research: Atmospheres 2003; 108(D22): 8851.
20. Koster RD, Suarez MJ. The influence of land surface moisture retention on precipitation statistics. Journal of Climate 1996; 9(10): 2551–2567.
21. Liang X, Wood EF, Lettenmaier DP. Surface soil moisture parameterization of the VIC-2L model: Evaluation and modification. Global and Planetary Change 1996; 13(1-4): 195–206.
22. Xia Y, Mocko D, Huang M, *et al.* Comparison and assessment of three advanced LSMs in simulating terrestrial water storage components over the U.S. Journal of Hydrometeorology 2017; 18: 625–649.
23. Keys RG. Cubic convolution interpolation for digital image processing. IEEE Transactions on Acoustics, Speech, and Signal Processing1981; 29(6): 1153–1160.
24. Carlson TN, Gillies RR, Perry EM. A method to

make use of thermal infrared temperature and NDVI measurements to infer surface soil water content and fractional vegetation cover. Remote Sensing Reviews 1994; 9(1-2): 161–173.
25. Sun DL, Kafatos M. Note on the NDVI-LST relationship and the use of temperature-related drought indices over North America. Geophysical Research Letters 2007; 34(24).
26. Cleveland WS. Robust locally weighted regression and smoothing scatterplots. Journal of the American Statistical Association 1979; 74(368): 829–836.
27. Reichle RH, Koster RD. Global assimilation of satellite surface soil moisture retrievals into the NASA Catchment land surface model. Geophysical Research Letters 2005; 32(2): L02404.
28. Anderson MC, Hain C, Otkin J, *et al*. An intercomparison of drought indicators based on thermal remote sensing and NLDAS-2 simulations with US Drought Monitor classifications. Journal of Hydrometeorology 2013; 14(4): 1035–1056.
29. Anderson MC, Hain C, Wardlow B, *et al.* Evaluation of drought indices based on thermal remote sensing of evapotranspiration over the continental United States. Journal of Climate 2011; 24(8): 2025–2044.
30. Anderson MC, Norman JM, Mecikalski JR, *et al.* A climatological study of evapotranspiration and moisture stress across the continental United States based on thermal remote sensing: 1. Model formulation. Journal of Geophysical Research: Atmospheres 2007; 112(D10).
31. Anderson MC, Norman JM, Mecikalski JR, *et al.* A climatological study of evapotranspiration and moisture stress across the continental United States based on thermal remote sensing: 2. Surface moisture climatology. Journal of Geophysical Research: Atmospheres 2007; 112(D11).
32. Norman JM, Kustas WP, Humes KS. Source approach for estimating soil and vegetation energy fluxes in observations of directional radiometric surface temperature. Agricultural and Forest Meteorology 1995; 77(3): 263–293.
33. Kogan FN. Global drought watch from space. Bulletin American Meteorological Society 1997; 78(4): 621–636.
34. Kogan FN. Application of vegetation index and brightness temperature for drought detection. Advanced Space Research 1995; 11: 91–100.
35. Wang P, Li X, Gong J, Song C. Vegetation temperature condition index and its application for drought monitoring. In Geoscience and Remote Sensing Symposium 2001; 1: 141–143.
36. Lorenz DJ, Otkin JA, Svoboda M, *et al*. Predicting the US Drought Monitor (USDM) using precipitation, soil moisture, and evapotranspiration anomalies. Part II: Intraseasonal drought intensification forecasts. Journal of Hydrometeorology 2017; 18: 1963–1982.
37. Grigg NS. The 2011–2012 drought in the United States: new lessons from a record event. International Journal of Water Resources Development 2014; 30(2): 183–199.
38. Otkin JA, Anderson MC, Hain C, *et al*. Assessing the evolution of soil moisture and vegetation conditions during the 2012 United States flash drought. Agricultural and Forest Meteorology 2016; 218: 230–242.
39. Hoerling M, Eischeid J, Kumar A, *et al.* Causes and predictability of the 2012 Great Plains drought. Bulletin of the American Meteorological Society 2014; 95(2): 269–282.
40. Sun D, Li Y, Zhan X, *et al*. Land surface temperature derivation under all sky conditions through integrating AMSR-E/AMSR-2 and MODIS/GOES observations. Remote Sensing 2019; 11(14): 1704.